Meteoritics & Planetary Science 39, Nr 7, 1223–1231 (2004)
Abstract available online at http://meteoritics.org

Chicxulub: Testing for post-impact hydrothermal input into the Tertiary ocean

A. J. ROWE, J. J. WILKINSON,* B. J. COLES, and J. V. MORGAN

Department of Earth Science and Engineering, Imperial College, London, SW7 2AZ, UK
*Corresponding author. E-mail: j.wilkinson@imperial.ac.uk

(Received 10 September 2003; revision accepted 27 April 2004)

Abstract–Studies of large terrestrial impact craters indicate that post-impact hydrothermal activity is a likely consequence of the crustal deformation and heating induced by such events. In the case of the Chicxulub basin, where marine conditions were re-established soon after the impact, significant fluxing of seawater through the crust and hydrothermal venting into the water column might be anticipated. We have carried out geochemical analyses of Tertiary carbonate sediments within the Yaxcopoil-1 (Yax-1) drill hole to test for evidence of such post-impact hydrothermal circulation. Hydrothermal activity is most likely to be found close to thick layers of melt rock inside the collapsed transient cavity, and it is estimated that Yax-1 is located ~20 km outside this cavity. Consequently, the most likely signature of hydrothermal venting into the water column would be geochemical anomalies attributable to fallout of suspended particulate matter from a submarine hydrothermal plume.

Samples of Tertiary biomicrites from depths of 794.01 to 777.02 m have high concentrations of manganese, iron, phosphorous, titanium, and aluminium and low iron/manganese ratios relative to samples from higher in the stratigraphic succession. This geochemical anomaly decreases fairly systematically between 793.13 m and 777.02 m, above which an abrupt change in geochemistry is observed. A mass balance calculation suggests that the anomaly is unlikely to be the result of a decreasing detrital input to the carbonate sediments and the nature of the element enrichments is consistent with expectations for fallout from a distal hydrothermal plume. We conclude that a post-impact hydrothermal system did develop at Chicxulub, which led to the expulsion of hydrothermal fluids into the Tertiary water column. Preliminary biostratigraphic and magnetostratigraphic dating on Yax-1 core suggest that this hydrothermal activity lasted for at least 300 ka.

INTRODUCTION

Hydrothermal fluid flow within impact craters plays a significant role in post-impact evolution; it can generate important mineral resources (e.g., Grieve and Masaitis 1994) and may influence the local biosphere (Pope et al. 2000). However, of the 160 or so known terrestrial impact craters (Grieve 1998), only a few have been the subject of detailed investigations into post-impact hydrothermal processes: Sudbury (Whitehead et al. 1992; Ames et al. 1998); Manson (McCarville and Crossey 1996); Haughton Dome (Osinski et al. 2001); Ries (Newsom et al. 1986); and Popigai, Kara, and Puchezh-Katunki (Naumov 2002). In the case of Sudbury, both magmatic segregation Ni-Cu ores and subsequent hydrothermal mineralization (Cu-PGE rich veins and Zn-Pb-Cu near-seafloor massive sulphides) formed as a direct result of the impact (Naldrett 1984; Rousell 1984).

The borehole Yaxcopoil-1 (Yax-1) has been drilled within the impact basin of the Chicxulub crater (Fig. 1) under the Chicxulub Scientific Drilling Program (CSDP). Core from this borehole has enabled an investigation into the existence of post-impact hydrothermal circulation in one of the largest craters on Earth.

Large impacts generate intense fracturing within the target rocks and produce large volumes of porous impact breccias and hot melt rocks, as well as significant uplift of hot basement within the central crater. Thus, large impact craters produce ideal conditions for extensive hydrothermal circulation. Immediately after impact, Chicxulub was located in an open marine shelf environment (Stinnesbeck et al. 2003) and any putative hydrothermal processes are likely to have been somewhat similar to those that occur at mid-ocean ridges (MOR). At MOR, cold seawater pervades the fractured crust and is heated by the thermal anomaly. The circulating fluids leach metals before buoyancy-driven flow back to the surface, where they may be vented into the water column (Campbell et al. 1988). A large proportion of the metals in such vent fluids precipitates close to the site of discharge. However, some of

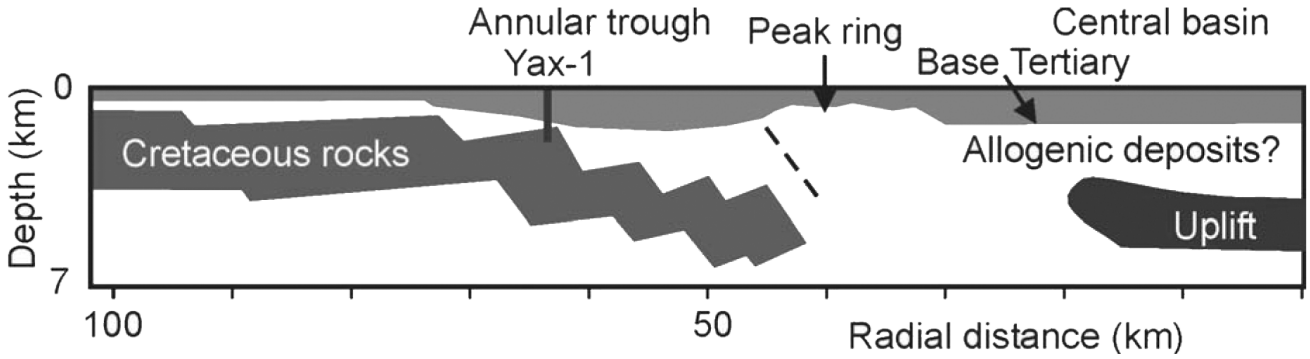

Fig. 1. A cartoon of the Chicxulub crater, redrawn from Morgan et al. (2002). Mapping of the Tertiary and Cretaceous rocks and of the peak ring is from offshore seismic reflection data. Structures within the central crater region are based on velocity data obtained from 3D tomographic seismic refraction data. Dashed line represents the interpreted location of the collapsed transient cavity. The Yax-1 drill-hole is plotted at the appropriate radial distance from the crater center. When projected onto the offshore seismic reflection data at the appropriate radial distance, Yax-1 is located in the outer edge of the annular trough.

the elements originally in solution are dispersed as a hydrothermal plume (Fig. 2). At the mid-Atlantic ridge the buoyant plume rises, entraining ambient seawater, until neutral buoyancy is achieved approximately 200 m above the site of venting, after which the plume spreads laterally (Rudnicki and Elderfield 1993; Mitra et al. 1994). Dissolved and particulate materials can be carried for several hundreds of km, before falling out of suspension to form metal-rich sediments.

Here, we present major and minor element analyses of a suite of Tertiary sediments from Yax-1, drilled within the southern annular trough of the Chicxulub impact crater, approximately 62 km from its center (Fig. 1). The aim of the study was to test the hypothesis that post-impact hydrothermal activity led to submarine venting of fluids within the Chicxulub impact basin and resulted in a hydrothermal particulate contribution to the Tertiary sedimentary succession.

Hydrothermal Systems

Most terrestrial impact craters exhibit some evidence of hydrothermal activity in the form of alteration, and open-space fracture fillings (e.g., Allen et al. 1982; McCarville and Crossey 1996). An extreme example is the 1850 Ma Sudbury structure, Ontario, where a regional impact-induced hydrothermal system developed at 1848.4 +3.8/−1.8 Ma, fuelled by heat produced by the Sudbury Igneous Complex (Ames et al. 1998). Evidence for extensive circulation of hydrothermal fluid includes vertically stacked, basin-wide, semi-conformable alteration zones, carbonate sinters on the palaeoseafloor and Zn-Cu-Pb replacement-type deposits (Ames et al. 1998).

Post-impact hydrothermal circulation in the Sudbury basin imposed a distinctive geochemical signature near the proposed vent site and within more distal sediments. Sedimentary rocks adjacent to the vent site are characterized by enrichment in Cu, Pb, Zn, Fe, and S, while the distal sediments exhibit anomalous Mn and Ba, which correlate with a marked depletion in sulphur (Whitehead et al. 1992). The overlying carbonaceous argillites contain a zone enriched in base metals and platinum group elements (PGE) over an area of 25 km^2, indicating that intermittent expulsion of hydrothermal fluids into the water column continued for some time during deposition of the post-impact sequence (Whitehead et al. 1992). The maximum duration of hydrothermal activity at Sudbury, implied by estimates of the rate of conductive cooling of the Sudbury igneous complex, is 1 Ma (Ames et al. 1998).

The geochemical patterns of element distribution in the Sudbury hydrothermal vent system are comparable to those in contemporary submarine hydrothermal systems at mid-ocean ridges (Fig. 2). The different geochemical processes operating in the near-vent and distal parts of the hydrothermal plume are reflected in the composition of proximal and distal hydrothermal sediments. Near-field sediments contain material directly precipitated from the vent fluid and/or material derived from weathering and mass wasting of seafloor hydrothermal sulphide deposits. These are characteristically enriched in Cu, Zn, Pb, Fe, and S, and have high Fe/Mn ratios of 900–2400 (German et al. 1990, 1999). Distal ridge-flank sediments show marked enrichment in Mn (with low Fe/Mn ratios) and REE (Ruhlin and Owen 1986), and have pronounced, negative Ce-anomalies (Bender et. al. 1971; Ruhlin and Owen 1986; Barrett and Jarvis 1988). Distal plume fallout also contributes elements transported as oxyanions such as P, Cr, V, As, and Se (Fig. 2).

The location of potential vent sites in relation to the Yax-1 drill-hole is not known, although they were likely to have been at least 20 km away, inboard of the inner edge of the collapsed transient cavity (Morgan et al. 2002; Fig. 1). Thus, in this study, we have focused on investigating possible geochemical anomalies that might be attributable to distal fallout from a hydrothermal plume.

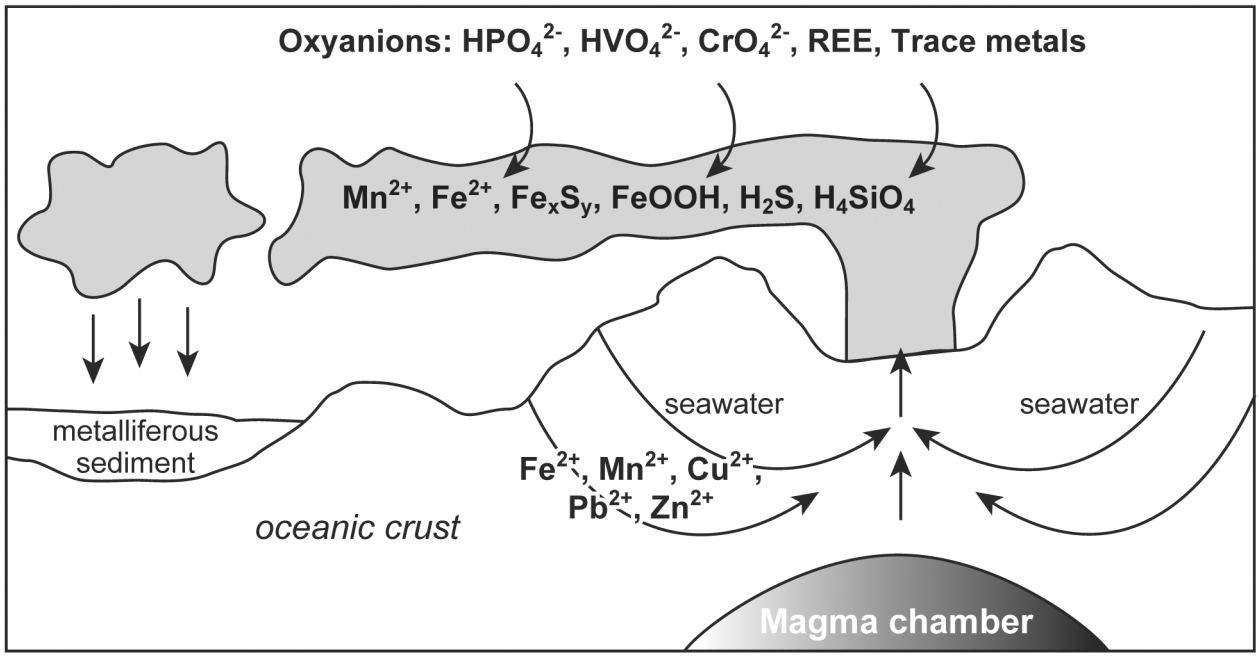

Fig. 2. Summary of main geochemical transport processes operating in contemporary mid-ocean ridge hydrothermal systems. Hydrothermal vent fluids from the east Pacific rise and mid-Atlantic ridge are typically enriched in Fe, Mn, Cu, Zn, Pb, Ni, Co, and H_2S. In all cases, fluids exhibit significant rare earth element (REE) enrichment and pronounced, positive Eu-anomalies (Michard et al. 1983; Michard and Albarede 1986; Campbell et al. 1988); some also show negative Ce-anomalies (German et al. 1990). Expulsion of such metal-rich fluids into overlying cold, alkaline seawater results in rapid precipitation of fine-grained, polymetallic sulphides and oxides (Mitra et al. 1994; German et al. 1999). Models suggest precipitation of Fe(II) by oxidation is initiated a few seconds later and oxyanions, such as HPO_4^{2-}, are co-precipitated with iron. Fe oxyhydroxide particles uptake dissolved trace elements by both co-precipitation and adsorption; co-precipitation occurs only in the buoyant plume, while adsorption occurs in the buoyant plume and the neutrally buoyant plume (Rudnicki and Elderfield 1993). As a result of this oxidative scavenging process, the concentration of trace elements, notably REE and P, in the neutrally buoyant plume increases with distance from the vent site (German et al. 1990). Mn oxyhydroxide particles may also scavenge REE from seawater. However, Mn is slow to oxidize, hence, Mn oxide particles are produced over longer time scales and occur in the distal part of the neutrally buoyant plume. The different geochemical processes operating in the near-vent part of the hydrothermal plume is reflected in the composition of proximal hydrothermal sediments. Near-field sediments contain material directly precipitated from the vent fluid and/or material derived from weathering and mass wasting of seafloor hydrothermal sulphide deposits. These are characteristically enriched in Cu, Zn, Pb, Fe, and S, have high Fe/Mn ratios (900–2400) and exhibit pronounced, positive Eu-anomalies (German et al. 1990, 1999).

SAMPLES AND ANALYTICAL METHODS

Twenty-three Tertiary carbonate samples from the Yax-1 drill-hole, ranging from 794.01 to 407.12 m in depth, were analyzed (Table 1). These comprise fine-grained, relatively homogeneous, cream-colored biomicrites, with fine horizontal laminations. Samples from 794.01 to 777.02 m contain 5–20% bioclasts, predominantly foraminifera and shell fragments, and 2% lithoclasts supported in a matrix of carbonate mud. Four phases of carbonate cement were identified using cathodoluminescence: 1) dedolomite rhombs; 2) interstitial sparry calcite cement; 3) prismatic, ferroan calcite surrounding bioclasts; and 4) anhedral Fe-poor calcite infilling bioclasts.

The lowermost sample, #329 (794.01 m), is just above the 2 cm-thick clay layer that forms part of the impact to post-impact transition sequence (Smit et al. 2004) that has been interpreted as the K-T boundary itself by Keller et al. (2004). Between samples #326 (777.02 m) and #327 (775.44 m) is the contact between a 7 m-thick carbonate massflow unit and overlying wackestones that marks a significant change in sediment geochemistry (see below). The nature of this boundary is uncertain, but the data reported here suggest that it is more important than a simple lithological contact and may represent an unconformity. From here up-section to 655.34 m, samples contain a greater proportion (20–60%) and wider variety of bioclasts, have less carbonate mud and higher porosity. Samples from 600.01 to 407.118 m are composed of 10–35% bioclasts, predominantly radiolarians, with a matrix of carbonate mud. No dolomite or dedolomite were observed in samples shallower than 781.61 m. None of the samples showed evidence of significant clastic input.

Due to the limited amount of material available (≤20 cc), samples were reduced to powder for geochemical analysis using an agate pestle and mortar. Sub-samples (0.1 g) were digested in PTFE test tubes, using a mixture of concentrated HNO_3/$HClO_4$/HF in a ratio of 2:1:5 ml (Thompson and Walsh 1983). The digests were evaporated to dryness and leached

Table 1. Chemical composition of Tertiary sediments (ppm).

Sample ID	Depth (m)	Al	Ba	Be	Ca	Co	Cu	Fe	K	La	Li
352	407.12	832.5	43.25	0.07	264900	<0.5	1.9	1687.5	<5.0	2.0	23
353	407.36	6500	21.75	0.165	239100	2.75	19.75	2805	1715	11.75	34.25
354	455.97	1932.5	31.5	0.11	285300	0.5	3.4	982.5	80	4.5	25.25
355	502.37	5432.5	850.75	0.21	249500	1.25	14.4	1790	1162.5	8.0	21.5
356	553.08	2815	18.25	0.18	129200	0.75	8.15	1020	100	3.0	9.0
364	600.01	3532.5	11.75	0.32	168400	1.5	12.1	1672.5	247.5	5.75	13.5
365a	655.34	497.5	28.75	0.055	298400	<0.5	2.25	410	<5.0	5.75	24.75
365b	655.34	582.5	31.75	0.055	295210	<0.5	2.3	500	<5.0	6.0	26
375	699.21	1265	64.5	0.075	298500	<0.5	6.5	657.5	180	6.75	26.75
357	757.77	740	6.0	0.04	290700	<0.5	2.45	642.5	60	4.75	24.25
327	775.44	1050	5.0	0.025	305600	<0.5	3.25	775	247.5	4.5	26
326	777.02	11510	107.5	0.27	251100	5.0	8.3	4000	3865	9.75	54
328	781.61	2495	17	0.08	295100	0.75	3.2	3275	1610	6.0	30.75
329	786.27	12910	89.25	0.325	247000	3.25	6.15	5255	4697.5	12.25	55.5
330	786.99	19840	75.5	0.515	191610	8.25	14.85	21400	5980	13.5	93.75
331	788.15	10060	38.25	0.265	248900	3.25	4.15	5217.5	3422.5	12.5	46.75
332	789.00	8710	47.5	0.22	265600	2.5	9.2	4495	3372.5	12	47.25
333	789.63	10900	56.5	0.25	241100	3.75	6.5	6015	4030	11	48
334	790.71	9310	38.25	0.19	258700	3.0	3.1	5835	3557.5	11.25	42.5
335	792.10	14040	41	0.28	231600	3.5	3.55	7810	5225	13.25	48
336	792.48	16620	47	0.325	224600	4.25	5.25	9995	5692.5	13.5	51.5
337	793.13	17380	46	0.33	231000	4.25	10.1	10130	7095	11.75	47.75
338	793.79	9577.5	27.25	0.205	255200	2.25	24.6	6015	4542.5	9.0	36.5
339a	794.01	7075	17.5	0.17	263500	2.5	11.1	5070	3477.5	8.25	34.5
339b	794.01	7102.5	17.5	0.17	257200	2.5	11.9	5110	3265	8.25	35
Precision (%)		16.1	9.9	n.d.[a]	3.5	n.d.[a]	9.2	20.6	12.6	4.3	6.4

Table 1. Chemical composition of Tertiary sediments (ppm). *Continued.*

Sample ID	Depth (m)	Mg	Mn	Mo	Na	Ni	P	Pb	S	Sr	Ti	V	Zn
352	407.12	n.d.	7.0	<0.5	3202.5	4.0	85	<3.0	605.5	1650	38.4	15	4.3
353	407.36	4981	8.5	1.75	7502.5	40.5	374	<3.0	3703	1094	188.9	39	57.7
354	455.97	6757	21.5	<0.5	3800	6.5	94	<3.0	755	1678	46.4	10	11.5
355	502.37	4276	16	0.75	5437.5	25	182	<3.0	2273	1348	106.1	36	37.6
356	553.08	1598	10	<0.5	5502.5	22.5	264	<3.0	1581	551	76.45	26	26
364	600.01	1832	29.5	0.5	5972.5	19	175	<3.0	1711	555.5	112.7	15	33.55
365a	655.34	3056	42	<0.5	7012.5	3.5	274	<3.0	615	360.75	17.3	3.0	7.1
365b	655.34	3108	40.5	<0.5	7160	3.0	298	<3.0	652.5	362.25	30.4	4.0	7.0
375	699.21	3168	62.5	1.5	6402.5	11.5	292	<3.0	1132	540	40.05	21	24.1
357	757.77	3516	119	0.5	6682.5	4.0	111	<3.0	692	334.5	25.85	15	4.4
327	775.44	4425	250	<0.5	3662.5	1.0	147	<3.0	439.5	241	45.85	3.0	12
326	777.02	13360	245	<0.5	6862.5	13	529	<3.0	674.5	383.5	603.9	12	15.3
328	781.61	5588	220.5	<0.5	4022.5	3.0	193	3.0	2457	290.5	106.3	4.0	9.4
329	786.27	14080	227.5	<0.5	6125	6.5	772	4.5	501	315.75	744.5	13	30
330	786.99	31160	320	<0.5	7185	15	664	3.0	11700	318.25	931.4	16	37.4
331	788.15	20340	399.5	<0.5	5235	6.0	567	<3.0	836	321	556.9	9.0	21.55
332	789.00	16710	354.5	<0.5	4670	6.5	444	<3.0	673.5	315.5	445.5	7.0	19.6
333	789.63	22880	397.5	<0.5	5097.5	9.5	562	4.5	537.5	301	617.3	10	27.95
334	790.71	19040	362	<0.5	4625	7.0	417	3.0	696	283.75	523.1	8.0	20
335	792.10	23500	369	<0.5	5370	8.0	548	<3.0	649	335	692.7	9.0	22.7
336	792.48	23940	343.5	<0.5	5855	10	680	3.0	727	405.25	1019	12	24.85
337	793.13	22070	349.5	<0.5	5740	9.5	643	<3.0	818.5	326	1004	14	22.4
338	793.79	16290	356	<0.5	4690	5.5	437	<3.0	813.5	382.5	491.1	7.0	17.65
339a	794.01	19950	426	<0.5	4055	44.5	412	<3.0	691	343.75	389.3	5.0	17.15
339b	794.01	20170	421.5	<0.5	4165	11.5	417	<3.0	697	344	389.6	5.0	16.45
Precision (%)		2.8	4.7	n.d.[a]	4.8	30.8	9.6	n.d.[a]	6.8	0.49	55.0	28.6	5.6

[a]n.d. = not determined.

for 1 h at 70 °C, using 2 ml of 4M HCl. Final solutions were made up with 8 ml of 0.3M HCl and stored in polystyrene centrifuge tubes. Major and minor elements were determined by inductively-coupled plasma atomic-emission spectrometry (ICP-AES) at the Natural History Museum, London.

In most cases, procedural blanks were below the instrumental detection limit. Where blanks were significantly greater than zero (95% confidence, student t-test) blank subtractions were carried out. These blanks were small (<5%) except where very low concentrations of analyte were present. To assess analytical bias, the international reference material BHVO1, the certified reference material NBS1C and in-house reference materials HRM1 and HRM2 were analyzed in duplicate. Generally, bias was less than 10% and is not considered significant in the present study where the relative changes in elemental concentrations are most important. Analytical precision, determined from duplicate sample analyses, was generally less than 10% (Table 1). One sample (330; 786.99 m) had anomalously high sulfur content (11,700 ppm) probably due to diagenetic pyrite and has therefore been excluded from the following discussion.

RESULTS

Results are presented in full in Table 1 and a selection of elements are plotted as a function of sample depth in Fig. 3. Between 794.01 m and 777.02 m, fairly systematic variations in chemical compositions are observed. Samples above a prominent mass flow unit at 784–777 m are geochemically distinct from those below (Fig. 3), and hence we separate our results and discussion into: Stage 1 (794.01–777.02 m) and Stage 2 (775.44–407.12 m).

Concentrations of manganese are high (340–425 ppm) in samples from 794.01 to 788.15 m (Fig. 3a). Concentrations decrease sharply above 788.15 m, but remain elevated (220–320 ppm) in samples from 786.99 to 775.44 m, before dropping rapidly to background levels (10–20 ppm). Iron and magnesium exhibit a similar pattern of abundance, decreasing gradually from high concentrations at 793.13 m within Stage 1 and showing uniformly low concentrations in the upper part of the section (Fig. 3a). Fe/Mn ratios are low for all samples in Stage 1 (12–29), decreasing slightly in parallel with Fe abundance. The ratio increases markedly in Stage 2, especially above 600.01 m, with values up to 328. Calcium, a good monitor of the total carbonate present, gradually increases through Stage 1 and then shows more variable concentrations in Stage 2, with particularly low concentrations (16.81, 12.89 wt%) observed at 600.01 m and 553.08 m, respectively.

With the exception of one high value for Cu in sample #338 (793.79 m), concentrations of Ni, Cu, and Zn are relatively low and show limited variation in the lower part of the section (Fig. 3b). In Stage 2, concentrations generally increase up-section and vary more significantly. These

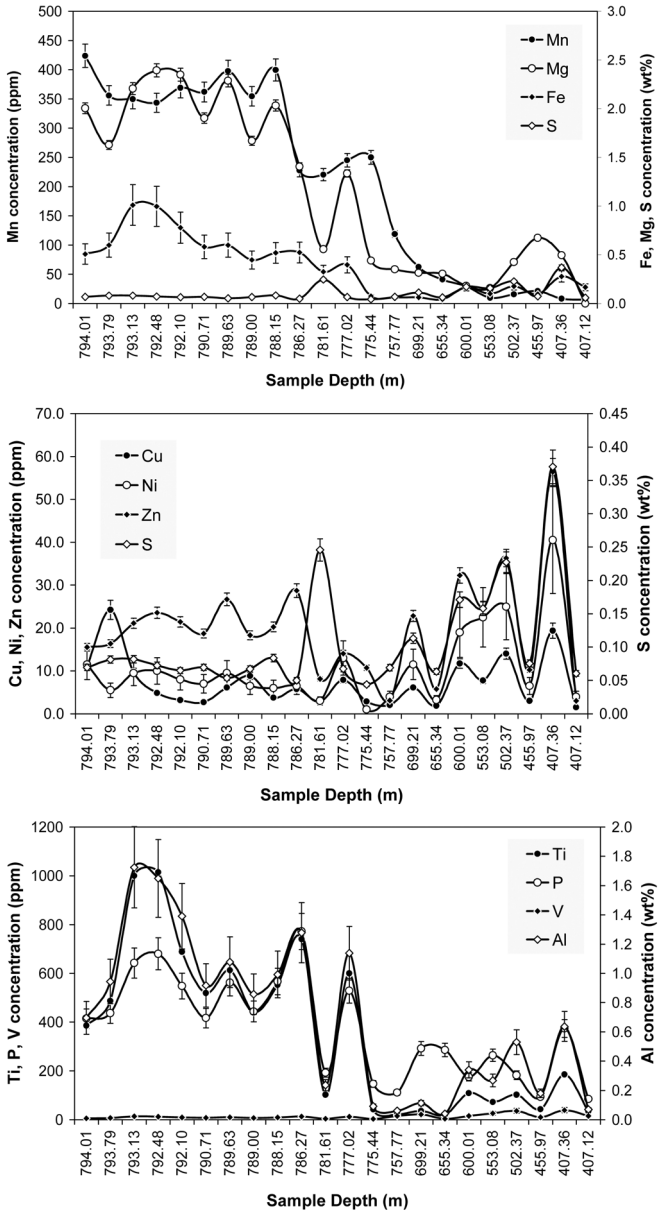

Fig. 3. Chemical compositions of Tertiary sediments from the Yax-1 drill hole plotted as a function of sample depth. Error bars indicate analytical precision and are smaller than the data symbols where not visible: a) Variations in Fe, Mn, Ca, and Mg; b) variations in Ni, Cu, Zn, and S; c) variations in Ti, Al, P, and V. Samples are plotted on a discrete x-axis because of the close sample spacing toward the base of the sampled interval.

patterns are rather similar to that displayed by sulfur, which is uniformly low in Stage 1 (with the exception of sample #328 [781.61 m]) and is higher and more variable in Stage 2 (440–3700 ppm; Fig. 3b). Statistical analysis of the relationship between sulfur and the chalcophile elements shows that there is no significant correlation between the two in Stage 1 (correlation coefficient, r = 0.212–0.554) but that there is a strong association in Stage 2 (r = 0.943–0.965). Principal component analysis (Howarth and Sinding-Larsen 1985) of

the Stage 2 data shows high loadings of V, Ni, Cu, Zn, Ba, and S in principal component 2, confirming a sulfur association of these elements that is absent in Stage 1.

The abundance patterns for Al, Ti, P, and V are very similar to each other (Fig. 3c), with very strong correlations in Stage 1 (r = 0.864 to 0.987) but less strong correlations in Stage 2 (r = 0.068 to 0.937). Concentrations are high in samples from 793.13 to 786.99 m, then decrease sharply to very low levels in Stage 2 in a similar fashion to Fe, Mg, and Mn. In the upper part of Stage 2, concentrations gradually increase to levels that are approximately half the average concentration in Stage 1.

DISCUSSION

Stage 1

The results for Stage 1 show that a number of elements (Mn, Fe, Mg, Ti, Al, P) generally decrease in concentration from the impact/post-impact transition upward through the Tertiary sedimentary sequence implying a causal link with the impact event. Correlation and principal component analyses show that Mn and Fe are associated with elements commonly occurring as oxyanions rather than Ca or S. This suggests Mn and Fe are largely present in an oxide form rather than substituted in carbonate or bound in sulfides. This, and the low Fe/Mn ratios (~10 to 30), are features consistent with the derivation of these elements from the distal part of a neutrally buoyant hydrothermal plume (Fig. 2). The trends for these elements are broadly comparable with those documented in sedimentary rocks distal to inferred hydrothermal vent sites in the Sudbury impact structure (Whitehead et al. 1992) and from modern distal hydrothermal sediments (German et al. 1999). These geochemical characteristics, and the absence of base metal (Cu, Pb, Zn) and S enrichment and metal-sulphur covariations in Stage 1, imply that any putative vent sites that could have sourced a hydrothermal component must have been located some distance (>25 km) from the site of the Yax-1 drill-hole.

The covariance between Fe and P (and possibly V) concentrations in Stage 1 can be explained by co-precipitation of P with Fe and/or scavenging of P from seawater by Fe oxyhydroxide hydrothermal plume particles as observed in contemporary submarine systems (Fig. 2). In addition, the good correlations of these elements with La suggests that the REE may have been scavenged from seawater by oxyhydroxides (cf., German et al. 1990). The abundance patterns of Al and Ti correlate closely with Fe and P, suggesting that these elements could also have been transported in plume particulates. However, Al and Ti are often considered to be indicators of detrital input, so this possibility is examined in more detail below.

Enrichment in Mg coincides with observations of dedolomite rhombs in CL petrographic analysis, which suggests Mg was originally present in these samples as dolomite. Dolomite formation may have been constrained by the nature of diagenetic processes operating during consolidation and burial of the sediment. However, given the correlation of Mg with Fe and Mn, it is plausible that dolomite only formed in samples from 794.01 to 781.61 m during diagenesis because excess Mg, derived from hydrothermal plume fallout, was available in the system.

Stage 2

In the upper part of the sequence (above 775.44 m), the trend of increasing base metal concentrations with decreasing sample depth is statistically correlated with sulfur concentrations, but there is no evidence of sulfide minerals that would indicate input from re-working of chimney or near-vent deposits. Therefore, the increased abundance of sulfur in the upper part of the sequence probably reflects higher rates of bacteriogenic sulphate reduction under different depositional conditions, with the chalcophile elements being fixed in diagenetic sulphides.

Evaluating Detrital Contributions

The trends of decreasing concentrations of trace elements such as Al in Stage 1 could be interpreted in terms of progressively decreasing clastic input to the depositional environment post K-T. However, there are two main lines of evidence to suggest that the elemental variations observed are not primarily controlled by this process.

First, it is known that early Tertiary sediments in the Chicxulub basin accumulated in a quiet open marine shelf environment (Stinnesbeck et al. 2003), with no evidence of significant clastic detritus. This is supported by our own petrographic observations, in which we did not identify a major clastic contribution to the carbonate sediments.

Second, a mass balance analysis of the geochemical data suggests that a detrital input alone cannot account for the data trends and that a separate component in the sediment, carrying high concentrations of Fe, Mn, Al, and Ti, is required. This analysis was carried out by assuming that Ca and Mg were solely contained in carbonate and calculating the non-carbonate fraction of each sample by subtraction. This yielded surprisingly high non-carbonate (largely detrital?) contributions of 24–36 wt% in the upper part of the sequence, with the proportion decreasing gradually up-section to 655.34 m (Fig. 4a). If Al is considered to reside only in detrital silicates, and the element/Al ratios of the detrital material remain constant through time, these ratios can be used to estimate elemental proportions contributed by the detrital component (cf., Cave et al. 2002). To do this, it is necessary to normalize the data and this was done relative to sample 777.02 m that marks the end of Stage 1 to assess whether variations in detrital input could account for the rather systematic decreases

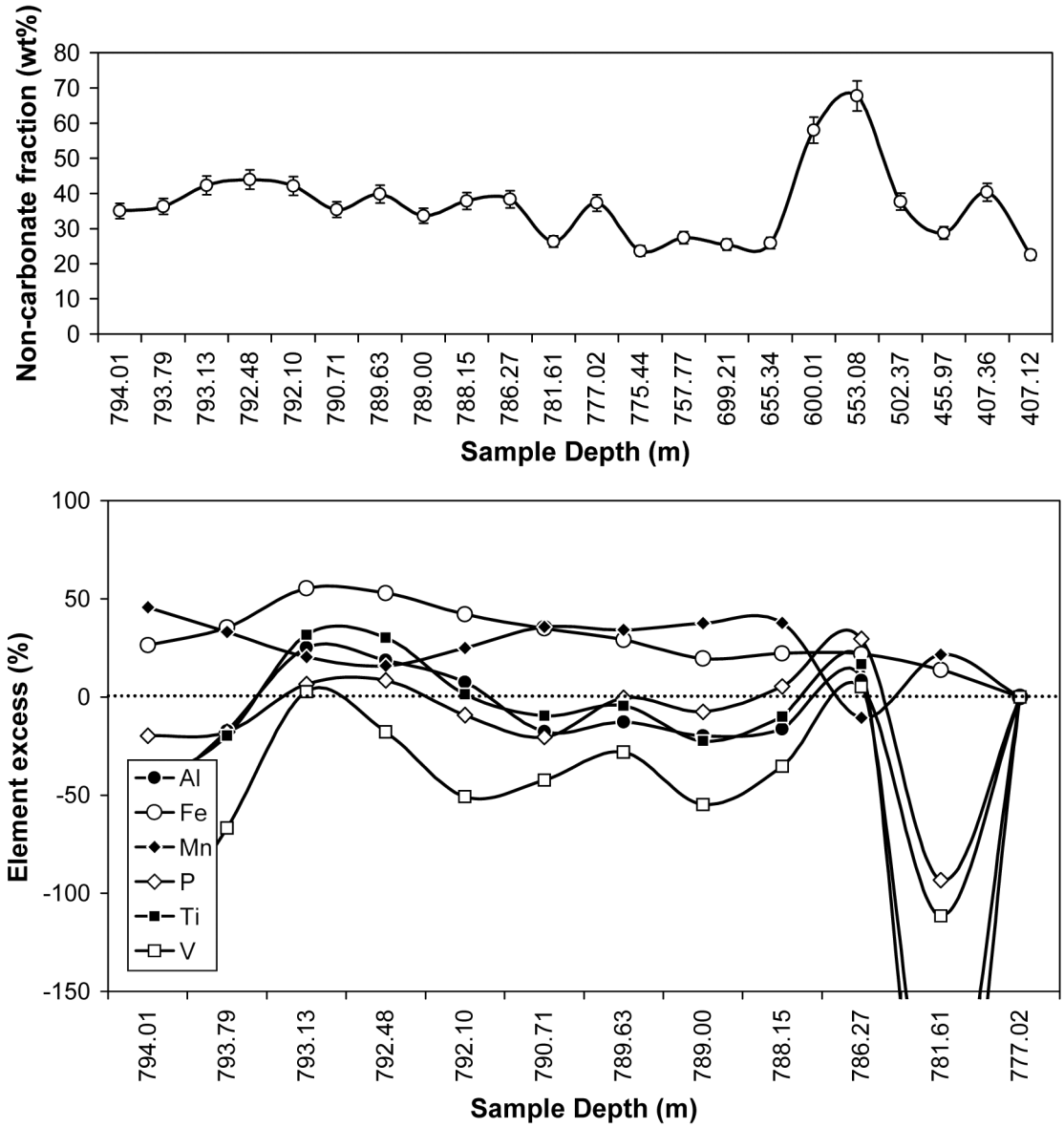

Fig. 4. Modeled effects of a possible detrital contribution: a) calculated non-carbonate contribution, assuming all Ca and Mg are present in carbonate. Error bars indicate propagated errors derived from analytical uncertainty in Ca and Mg; b) calculated elemental excess that cannot be attributed to a detrital contribution to the non-carbonate component in the lower part of the sequence, assuming Al is only present in detrital material and the composition of detrital material does not vary. Calculated excess concentrations from the upper part of the sequence (not shown) are generally large and negative indicating a significant change in composition of the non-carbonate fraction.

in element concentrations observed in Stage 1. However, it is important to note that the normalization point has no effect on the relative trends observed.

The results of this analysis are shown in Fig. 4b., plotted in terms of the elemental excesses that cannot be attributed to the inferred detrital component. This modeling shows that the apparent slight decrease in the detrital component through time in Stage 1 (Fig. 4a) is insufficient to account for the magnitude of the decreases observed for Fe and Mn, and also Ti and Al in the lower part of the sequence. However, variations in detrital content can account for much of the decrease seen in P. In combination with the strong inter-element correlations and likely oxide association, this implies that the Fe, Mn, and other elemental anomalies observed in Stage 1 are attributable to a separate (non-detrital, non-carbonate) source that diminishes with time, consistent with derivation from a hydrothermal plume. The dramatic differences observed in the calculated elemental excesses in Stage 2 serve to highlight the contrasting geochemical character of Stage 2 sediments. The large negative shifts are attributable to a non-carbonate component of markedly different composition to Stage 1, very poor in Al, Ti, Fe, and

Mn. This change coincides with the appearance of radiolarians in samples from 699.21 m to 502.37 m and is, therefore, due in part to a greater content of siliceous microfossils.

Duration of Hydrothermal Inputs

Geochemical anomalies attributable to hydrothermal plume fallout are observed between depths of 794.01 and 777.02 m. Results from biostratigraphic and magnetostratigraphic studies of the Yax-1 drill hole samples can be used to constrain the duration of the inferred post-impact hydrothermal inputs. Assuming that these anomalies have not been significantly dispersed by bioturbation or diagenetic remobilization, their stratigraphic extent can be used to estimate the time period over which hydrothermal activity occurred. Tertiary planktic foraminifera from zone P1a(2) first appear at 794.11 m, and zone P1c fossils are observed above 794.05 m (Keller et al. 2004). An interpretation of the magnetostratigraphic analyses places a switch from magnetochron 29R to 29N between 794.04 and 794.08 m (Rebolledo-Vieyra et al. 2004). Both these observations suggest that the sediments at ~794.05 m were deposited ~300 ka after the K-T boundary. P2 planktic foraminifera, which have an age of ~3.5 Ma post K-T (e.g., Berggren et al. 1995), are first observed at ~792 m by Arz et al. (2004) and at 789.2 m by Stinnesbeck (2003, personal communication). However, we note that these interpretations are preliminary and dating of the Paleocene section is still in progress. Our initial conclusion is that hydrothermal processes were active in the Chicxulub basin for at least 300 ka, and could have been operative for significantly longer.

CONCLUSIONS

The geochemical anomalies observed in samples from 794.01 to 786.99 m in the Yax-1 drill-hole, such as enrichment in Mn, Fe, and P, and low Fe/Mn ratios, are consistent with the input of particulate material from distal hydrothermal plume fallout. Therefore, we suggest that post-impact hydrothermal activity led to submarine venting of fluids within the Chicxulub impact basin during the deposition of early Tertiary sediments. However, no evidence exists that Yax-1 is in the proximity of a vent site.

The presence of a post-impact hydrothermal system in the Chicxulub basin would have important implications. Although there is no indication of mineralization in the samples analyzed, the submarine venting of hydrothermal fluids opens up the possibility that base metal sedimentary-exhalative deposits may have formed elsewhere in the basin. The hydrothermal system also may have been sufficiently long-lived (>300 ka) to allow the development of vent-related ecosystems within the impact crater. Such systems could have acted as important refuges for organisms in the post K-T ocean.

Acknowledgments–We thank Lizzie Morris for sample preparations and Helen Crowther for laboratory assistance. This work forms part of the MSci dissertation of AJR, supported by the Department of Earth Science and Engineering at Imperial College London and the Joint Analytical Facility of the Department of Earth Science and Engineering and the Natural History Museum, London. We thank the International Continental Drilling Program for funding the drilling of Yaxcopoil-1, and Jaime Urrutia-Fucugauchi and Ana Maria Soler-Arechalde for overseeing the core sampling at Universidad Nacional Autónoma de México.

Editorial Handling—Dr. Dieter Stöffler

REFERENCES

Allen C. C., Gooding J. L., and Klaus K. 1982. Hydrothermally altered impact melt rock and breccia: Contributions to the soil of Mars. *Journal of Geophysical Research* 87:10083–10101.

Ames D. E., Watkinson D. H., and Parrish R. R. 1998. Dating of a regional hydrothermal system induced by the 1850 Ma Sudbury impact. *Geology* 26:447–450.

Arz J. A, Alegret L., and Arenillas I. 2004. Foraminiferal biostratigraphy and paleoenvironmental reconstruction at Yaxcopoil-1 drill hole, Chicxulub crater, Yucatán Peninsula. *Meteoritics & Planetary Science*. This issue.

Barrett T. J. and Jarvis I. 1988. Rare earth element geochemistry of metalliferous sediments from DSDP Leg 92, the East Pacific Rise transect. *Chemical Geology* 67:243–259.

Bender M., Broeker W., Gornitz V., Middel U., Kay R., Sun S. S., and Biscaye P. 1971. Geochemistry of three cores from the East Pacific Rise. *Earth and Planetary Science Letters* 12:4250–433.

Berggren W. A., Kent D. V., Swisher C. C., III, and Aubry M. P. 1995. A revised Cenozoic geochronology and chronostratigraphy. In *Geochronology, time, and global stratigraphic correlation,* edited by Berggren W. A., Kent D. V., Aubry M. P., and Hardenbol J. Special Publication 54. Tulsa: Society of Economic Geologist and Paleontologist. pp. 129–212.

Campbell A. C., Palmer M. R., Klimkhammer G. P., Bowers T. S., Edmond J. M., Lawrence J. R., Casey J. F., Thompsen G., Humphries S., Rona R., and Karson J. A. 1988. Chemistry of hot springs on the Mid-Atlantic Ridge. *Nature* 335:514–519.

Cave R. R., German C. R., Thomson J., and Nesbitt R. W. 2002. Fluxes to sediments underlying the Rainbow hydrothermal plume at 36°14′N on the Mid-Atlantic Ridge. *Geochimica et Cosmochimica Acta* 66:1905–1923.

German C. R., Klinkhammer G. P., Edmond J. M., Mitra A., and Elderfield H. 1990. Hydrothermal scavenging of rare earth elements in the ocean. *Nature* 345:516–518.

German C. R., Hergt J., Palmer M. R., and Edmond J. M. 1999. Geochemistry of a hydrothermal sediment core from the OBS vent field, 21°N, East Pacific Rise. *Chemical Geology* 155:65–75.

Grieve R. A. F. and Masaitis V. L. 1994. The economic potential of terrestrial impact craters. *International Geological Reviews* 36: 105–151.

Grieve R. A. F. 1998. Extraterrestrial impacts on Earth: The evidence and the consequences. In *Meteorites: Flux with time and impact effects,* edited by Grady M. M., Hutchinson R., McCall G. J. H., and Rothery D. A. Special Publication 14. London: Geological Society of London. pp. 105–131

Howarth R. J. and Sinding-Larsen R. J. 1985. Multivariate analysis.

In *Handbook of exploration geochemistry, statistics, and data analysis in geochemical prospecting,* edited by Howarth R. J. New York: Elsevier. pp. 207–289.

Keller G., Adatte T., Stinnesbeck W., Rebolledo-Vieyra M., and Urrutia-Fucugauchi J. 2004. Chicxulub impact predates the K-T boundary mass extinction. *Proceedings of the National Academy of Sciences* 101:3753–3758.

McCarville P. and Crossey L. J. 1996. Post-impact hydrothermal alteration of the Manson impact structure. In *The Manson impact structure, Iowa; Anatomy of an impact crater,* edited by Koeberl C. and Anderson R. R. Special Paper 302. Boulder: Geological Society of America. pp. 347–376.

Michard A. and Albarede F. 1986. The rare earth content of some hydrothermal fluids. *Chemical Geology* 55:51–60.

Michard A., Albarede F., Michard G., Minster J. F., and Charlou J. L. 1983. Rare earth element and uranium variation in high temperature hydrothermal solutions from the East Pacific Rise hydrothermal vent field (13° N). *Nature* 303:795–797.

Mitra A., Elderfield H., and Greaves M. J. 1994. Rare earth elements in submarine hydrothermal fluids and plumes from the Mid-Atlantic Ridge. *Marine Chemistry* 46:217–235.

Morgan J. V., Warner M. R., and Grieve R. A. F. 2002. Geophysical constraints on the size and structure of the Chicxulub impact crater. In *Catastrophic events and mass extinctions: Impacts and beyond,* edited by Koerberl C. and MacLeod K. G. Special Paper 356. Boulder: Geological Society of America. pp. 39–46.

Naldrett A. J. 1984. Mineralogy and composition of the Sudbury ores. In *The geology and ore deposits of the Sudbury structure,* edited by Pye E. G., Naldrett A. J., and Giblin P. E. Special Volume 1. Toronto: Ontario Geological Survey. pp. 309–325.

Naumov M. V. 2002. Impact-generated hydrothermal systems; data from Popigai, Kara, and Puchezh-Katunki impact structures. In *Impacts in Precambrian shields,* edited by Plado J. and Pesonen. L. J. Impact Studies Series. Berlin: Springer. pp. 117–171.

Newsom H. E., Graup G., Seward T., and Keil K. 1986. Fluidization and hydrothermal alteration of the suevite deposit in the Ries Crater, West Germany, and implications for Mars. *Journal Geophysical Research* 91:239–251.

Osinski G. R., Spray J. G., and Lee P. 2001. Impact-induced hydrothermal activity within the Haughton impact structure, Arctic Canada; generation of a transient, warm, wet oasis. *Meteoritics & Planetery Science* 36:731–745.

Pope K. O., Ames D. E., Kieffer S. W., and Ocampo A. C. 2000. Impact crater hydrothermal niches for life on Mars: A question of scale (abstract #6068). In *Concepts and approaches for Mars exploration,* edited by Hubbard S. LPI Contribution No 1062. Houston: Lunar and Planetary Institute.

Rebolledo-Vieyra M. and Urrutia-Fucugauchi J. 2004. Magnetostratigraphy of the impact breccias and post-impact carbonates from borehole Yaxcopoil-1, Chicxulub impact crater, Yucatán, Mexico. *Meteoritics & Planetary Science* 39:821–829.

Rousell D. H. 1984. Mineralization in the Whitewater Group. In *The geology and ore deposits of the Sudbury structure,* edited by Pye E. G., Naldrett A. J., and Giblin P. E. Special Volume 1. Toronto: Ontario Geological Survey. pp. 219–232.

Rudnicki M. D. and Elderfield H. 1993. A chemical model of the buoyant and neutrally buoyant plume above the TAG vent field, 26 degrees N, Mid-Atlantic ridge. *Geochimica Cosmochimica Acta* 57:2939–2957.

Ruhlin D. E. and Owen R. M. 1986. The rare earth element geochemistry of hydrothermal sediments from the East Pacific Rise, examination of a seawater scavenging mechanism. *Geochimica Cosmochimica Acta* 50:393–400.

Smit J., van der Gaast S., and Lustenhouwer W. 2004. Is the transition impact to post-impact rock complete? Some remarks based on XRF scanning, electron microprobe, and thin section analyses of the Yaxcopoil-1 core in the Chicxulub crater. *Meteoritics & Planetary Science.* This issue.

Stinnesbeck W., Keller G., Adatte T., Harting M., and Stüben D. 2003. Yaxcopoil-1 and the Chicxulub impact (abstract #4037). In *Large meteorite impacts,* LPI Contribution No 1167. Houston: Lunar and Planetary Institute.

Thompson M. and Walsh J. N. 1983. *A handbook of inductively coupled plasma spectrometry.* New York: Chapman and Hall. 273 p.

Whitehead R. E. S., Davies J. F., and Goodfellow W. D. 1992. Lithogeochemical patterns related to sedex mineralization, Sudbury Basin, Canada. *Chemical Geology* 98:87–101.